1 2 First-principles study of FeO₂H_x solid and melt system at high pressures: Implications for ultra-low velocity zones 3 Authors: Jie Deng^{1*}, Bijaya B. Karki², Dipta B. Ghosh², and Kanani K. M. Lee¹ 4 5 **Affiliations:** 6 ¹Department of Geology and Geophysics, Yale University, New Haven CT 06511 7 ²School of Electrical Engineering and Computer Science, Department of Geology and 8 Geophysics, and Center for Computation and Technology, Louisiana State University, Baton Rouge, Louisiana 70803, USA 9 10 **Corresponding author:** Jie Deng (jie.deng@yale.edu) 11 **Key Points: (140 characters or less with no special characters or punctuation)** 12 Pyrite-type FeO₂H_x is likely to be melted near the core-mantle boundary 13 The seismic velocity of liquid FeO₂H is much lower than pyrite-type FeO₂H solid A molten FeO₂H_x induced ultra-low velocity zone requires high viscosity and/or 14 15 vigorous convection 16 17 18 19

Abstract (150)

Pyrite-type FeO_2H_x (P phase) has recently been suggested as a possible explanation for ultra-low velocity zones (ULVZs) due to its low seismic velocity and high density. Here we report the results on the congruent melting temperature and melt properties of P phase at high pressures from first-principles molecular dynamics simulations. The results show that P phase would likely be melted near the core-mantle boundary. Liquid FeO_2H_x has smaller density and smaller bulk sound velocity compared to the isochemical P phase. As such, small amounts of liquid FeO_2H_x could account for the observed seismic anomaly of ULVZs. However, to maintain the liquid FeO_2H_x within the ULVZs against compaction requires special physical conditions, such as relatively high viscosity of the solid matrix and/or vigorous convection of the overlying mantle.

Plain Language Summary (200)

Ultra-low velocity zones (ULVZs) are 5-40 km thick patches lying above Earth's core-mantle boundary (CMB). They are characterized with anomalously low seismic velocities compared with the ambient mantle and may contain important clues on the thermochemical evolution of the Earth. A recent experimental study argued that ULVZs may be caused by the accumulation of pyrite-type FeO₂H_x (P phase) at the bottom of the mantle. Here, for the first time, we systematically study the thermoelastic properties of both FeO₂H_x solid and liquid phases. We found that P phase is likely melted near the CMB and thus cannot be the source of ULVZs. Furthermore, in order for the molten product of P phase to cause ULVZs, the dense and nearly inviscid melts must be dynamically stable and confined within the ULVZs, which requires that the mantle is highly viscous and/or convects vigorously. As P phase is an important high-pressure volatile bearing phase, our study also sheds lights on the role of FeO₂H_x system in the deep circulation of hydrogen and oxygen within the Earth.

1. Introduction

Ultra-low velocity zones (ULVZs) are 5–40 km thick patches lying directly above the core–mantle boundary (CMB), where seismic wave speeds are depressed by ~10% for P-waves and 10%–30% for S-waves (Williams & Garnero, 1996). Several mechanisms have been proposed to explain ULVZs, including the oft-cited partial melting (Williams & Garnero, 1996) and solid-state iron-enriched materials (Mao et al., 2006; Wicks et al., 2010; Brown et al., 2015). The different mechanisms correspond to distinctive thermal and chemical states of the CMB resulting from different Earth evolution scenarios. Careful assessment of the different proposed mechanisms including the compositional likelihood and stability field at such depths, therefore, becomes necessary to distinctively pinpoint the actual origin(s) of ULVZs.

Very recently, pyrite-type $FeO_2H_x(x = 0-1)$, named P phase hereafter) has been invoked as a plausible cause of ULVZs (Liu et al., 2017). Based on their laser-heated diamond-anvil cell experimental results, Liu et al. (2017) suggested that the pyrite-type iron peroxide with varying hydrogen concentration is stable up to 2600 K and 133 GPa while exhibiting thermoelastic properties consistent with ULVZs. The temperature near the CMB is, however, generally expected to reach ~4000 K at 136 GPa (Anderson, 2002). Under such extreme conditions, the stability of P phase remains unclear. The comparison with the melting behavior of FeO may shed light on this issue. The melting temperature of FeO at the CMB is around 3700 K (Fischer & Campbell, 2010) and falls into the lower end of the proposed CMB temperature (Nomura et al., 2014; Andrault et al., 2016). The P phase contains more light elements and thus may be less refractory as the addition of hydrogen usually tends to lower the melting temperatures of the system (e.g., Nomura et al., 2011). Therefore, P phase might melt at the lowermost mantle.

If P phase melts near the CMB, the resulting melt may have very different seismic and dynamic properties. To assess the (solid/liquid) phase stability of FeO_2H_x composition at the CMB, we calculate the melting temperatures of the two end members of P phase, i.e., FeO_2 and FeO_2H , from first-principles molecular dynamics (FPMD) simulations. Thereafter, we evaluate the thermoelastic properties of liquid FeO_2H_x and further examine whether it could be the source material for ULVZs.

2. Computational Methodology

Our FPMD simulations are based on density functional theory and projector augmented wave method as implemented by Vienna Ab initio Simulation Package (VASP) (Blöchl et al., 1994; Kresse & Joubert, 1999). While we used the generalized gradient approximation (GGA) for the exchange-correlations functional (Perdew et al., 1996), we also explored the effects of the Hubbard term with U = 5 eV and J = 0.8 eV (Jang et al., 2017) and local density approximation (LDA). The plane-wave cut-off was set at 400 eV (which resulted in Pulay stress of about 10 GPa) and Brillouin zone sampling was performed at the Gamma point. The time step was set at 0.5 to 1 fs and the allowed error in total energy was set between 10^{-4} - 10^{-6} eV. The run durations varied from 5 to 20 ps. The supercells contained Fe₃₂O₆₄, Fe₃₂O₆₄H₃₂, and Fe₁₆O₃₂H₈₀.

To calculate the melting temperatures of FeO₂H and FeO₂ at high pressures, we used the Z method, which is based on the notion that the internal energy of the crystal at the superheating limit equals that of the isochemical liquid at the melting temperature (Belonoshko et al., 2006). It has been previously used in multiple melting studies (Belonoshko & Rosengren, 2012; Wang et al., 2013; Li et al., 2014; González-Cataldo et al., 2016). We performed FPMD simulations in the microcanonical (NVE) ensemble on a single solid system at different initial energies controlled by the initial temperature set in each simulation. When the crystal is heated beyond its overheating limit, the temperature naturally drops to the melting temperature as the latent heat is removed from the kinetic energy. The connected P-T points on the isochore form a Z-shaped curve. Several simulations for each isochore are needed in order to yield a single accurate melting temperature (Figures 1 and S1). The Z method only works for congruent melting because it compares the internal energy variation of an isochemical solid and liquid. FeO₂ may melt congruently while FeO₂H may melt incongruently as discussed in detail in the following section. Nevertheless, the calculated "congruent melting temperature" of FeO₂H informs how the addition of hydrogen would affect the melting temperature of the FeO_2H_x system. To study the equation of state of FeO_2H_x solid and liquid, we then performed several FPMD simulations in the canonical (NVT) ensemble. We confirmed the physical state (solid or liquid) of the simulated system by examining the partial radial distribution functions (Figure S2) and atomic trajectories (Figure S3). We also found that running longer simulations (> 20 ps) and doubling supercell (Fe₆₄O₁₂₈) did not affect the calculated results significantly, for instance, final pressure and temperature from our NVE runs varied by less than 0.2 GPa and 100 K, respectively.

93 94

95

96

97

98

99

100

101

102

103

104

105

106

107

108

109

110

111112

113114

115

116

117

118

119

120

121

122123

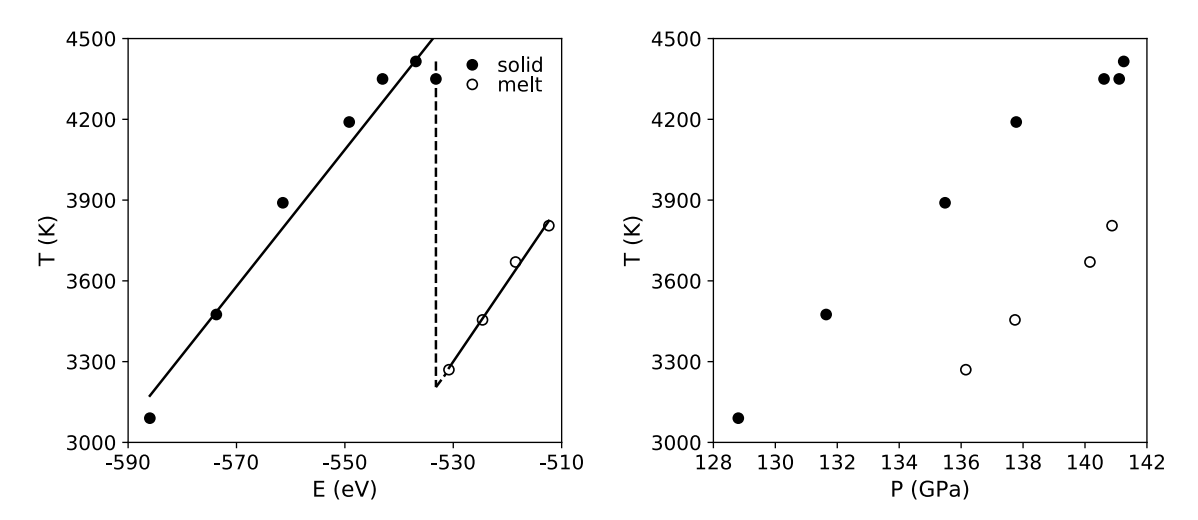


Figure 1. (A) The Z isochores in temperature-total energy and (B) temperature-pressure domains for pyrite-type FeO₂. The lower bound of the melting temperature (3205 K) is taken as the temperature at which the total energy of the liquid equals the maximum total energy of the solid reached in the simulation (the intersection of the vertical dashed line and the liquid branch). The lowest temperature of the melt (3275 K) is taken as the upper bound of the melting temperature.

3. Results and Discussion

3.1. Melting temperatures

The congruent melting temperatures of FeO₂ and FeO₂H were calculated near CMB pressures as summarized in Figure 2. For FeO₂, the melting temperature using GGA increases from 3020±30 K at 117 GPa to 3415±80 K at 156 GPa, in good agreement with the previous calculation (Zhang et al., 2017). For FeO₂H, the melting temperature using GGA is in agreement with He et al. (2018) at 118 GPa but not at higher pressures. Note that He et al. (2018) estimated the boundary between the melt/solid FeO₂H by simulating at widely spaced P-T conditions, which cause the zigzag melting boundary and the apparent discrepancy with our results. The calculated melting temperatures of FeO₂ are lower than the experimental FeO melting curve (Fischer & Campbell, 2010), as one would expect intuitively. Our results show that FeO₂H melts at lower temperatures at the pressures investigated, which implies that adding H into FeO₂ further lowers the melting temperature when compared to FeO. For the sake of comparison, we have also estimated the melting temperatures both by GGA+U and LDA. The values are shifted upwards by 200 to 300 K (Figure 2). To elaborate, because LDA tends to over-bind, it results in higher melting temperature in comparison to GGA. Similarly, although no data on the effects of U on the melting temperatures exist, the penalty function U in GGA+U is known to increase the transition (structural and spin) pressures (Ghosh & Karki, 2016). Irrespective of the choice (i.e., LDA, GGA or GGA+U), our results (Figure 2) suggest that FeO_2H_x systems are likely to be molten near the CMB.

The FPMD simulations put meaningful constraints on the melting temperature of P phase. We note that our predicted congruent melting temperature of P phase falls very close to one experimental data point (125 GPa, 3100-3300 K) which observed solid-state FeO_2H_x for x = 0.5-0.7 (Liu et al., 2017). There are a couple of possible reasons why P phase was observed at such high temperatures. First, large temperature gradients likely existed in LHDAC experiments and as such, accurate temperature measurement is difficult (Deng et al., 2017) especially for flash heating. Second, if the kinetics of melting is slow, P phase may be metastable at temperatures higher than its melting temperature given the short flash heating durations.

Comparison between the melting temperatures of FeO₂ and FeO₂H with mantle geotherms together with high-pressure experiments (e.g., Liu et al., 2017; Yuan et al., 2018) suggests that P phase is thermally stable (not melted) in most of the mantle (Brown & Shankland, 1981; Anderson, 1982, 2002). However, this may not be the case in the lowermost mantle and within the thermal boundary layer right above the CMB where mantle temperatures drastically increase by \sim 1000 K within less than 200 km (Anderson, 2002). The congruent melting curve of P phase likely intersects with the geotherm, indicating the onset of melting. The exact depth at which melting can occur depends on the hydrogen content and the mantle temperature profile. No matter where within the

thermal boundary layer melting occurs, P phase is not thermally stable within the ULVZs that are characterized by CMB temperatures.

The above discussion is based on the assumption that P phase melts congruently. However, as mentioned earlier, P phase may not melt congruently. Nishi et al. (2017) argued that P phase would dissociate into post-perovskite type Fe₂O₃ and H₂O above 2400 K at lowermost mantle pressures. This is in contrast to the experiments (Hu et al., 2017; Liu et al., 2017) where P phase is found to be stable at temperatures as high as 3100-3300 K (Figure 2). On the other hand, a recent first-principles study computed the Gibbs free energies of the decomposition reactions of FeO₂ (FeO₂ = Fe₂O₃ + O₂) between 40-80 GPa and up to 2400 K and found that this reaction is not energetically favorable at high pressures (>40 GPa) (Tang et al., 2018), supporting the experimental observations by Hu et al. (2017) and Liu et al. (2017). Another static first-principles study suggested that at lowermost mantle conditions, the dehydrogenation dissociation (FeO₂H = FeO₂H_x + $\frac{(1-x)}{2}$ H₂) of pyrite-type FeO₂H is energetically unfavorable while the dehydration dissociation (2FeO₂H = Fe₂O₃ + H₂O) may be energetically accessible, in agreement with (Nishi et al., 2017).

If P phase (including FeO_2 and FeO_2H_x (x>0)) melts incongruently, the incongruent melting products may be FeO₂H_x, FeO₂, Fe₂O₃, H₂O, H₂, and O₂ according to the discussion above. Unlike congruent melting, the melting temperature of P phase needs be further subdivided into the solidus melting temperature and the liquidus melting temperature, both of which are related to the endmember melting temperatures and mixing properties. Due to the lack of mixing parameters between end members (FeO₂, Fe₂O₃, H₂O, H₂, and O₂) at CMB conditions, we consider only ideal mixing. In this case, the solidus and liquidus melting temperatures of P phase range from the lowest melting temperatures to the highest melting temperatures of the end members. In other words, the melting temperatures of H₂O or H₂ or O₂ likely constrain the lower bound of the solidus/liquidus temperatures (Lin et al., 2005; Deemyad & Silvera, 2008) while those of iron-bearing (e.g., FeO₂, Fe₂O₃) compound likely constrain the upper bound. Here we focus on the upper bound of the solidus/liquidus to examine whether P phase would melt completely near the CMB. The upper limit of calculated congruent melting temperature of the FeO₂ (i.e., LDA or GGA+U) at CMB is ~3450 K. Assuming a linear relationship between the melting temperature and O content for FeO_x system, the post-perovksite phase of Fe₂O₃ melts at 3350–3690 K at 136 GPa, which still falls in the lower end of the estimated CMB temperatures (Figure 2).

The incorporation of other elements (e.g., Al, Si, Mg) may also affect melting of P phase. A recent experimental study found that (Fe,Al)O₂H (the solid solution phase of AlO₂H and FeO₂H) is stable at 107-136 GPa and 2400 K (Zhang et al., 2018). AlO₂H is likely more refractory than FeO₂H (He et al., 2018) and the incorporation of Al in P phase could increase its melting temperature. However, the degree of this enhancement is unknown. Also, the amount of AlO₂H phase available at the lowermost mantle is likely very limited (Mashino et al., 2016). In contrast, P phase could be relatively abundant by the reaction of core materials and the water brought by subduction from the crust and the primordial water in the mantle (Hallis et al., 2015; He et al., 2018) proposed by (Liu et al.,

2017; Mao et al., 2017). As such, the (Fe,Al)O₂H solid solution at CMB may be very diluted in AlO₂H component and the melting temperature would not be very different from pure P phase discussed above. In addition to Al, dissolving other elements such as Mg and Si may also increase the melting temperature of P phase. However, whether or not those reactions are energetically favorable need to be investigated.

To sum up, the solid P phase is likely to melt (completely) in the lowermost mantle even if the P phase melts incongruently or if P phase forms solid solution with AlO₂H. Consequently, P phase cannot be the source of ULVZs.



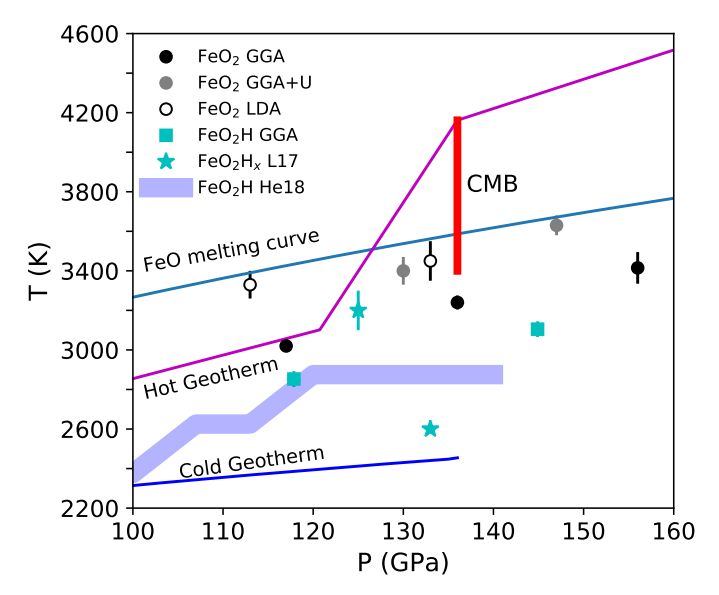


Figure 2. Congruent melting temperatures of FeO₂ (solid circles) and FeO₂H (solid squares) using GGA at high pressures (with the GGA+*U* and LDA results shown for FeO₂ by grey and open circles, respectively). Two high-temperature experimental data where P phase is observed are plotted as asterisks (Liu et al., 2017) and the FeO melting curve is taken from (Fischer & Campbell, 2010). The thick blue zigzag curve is the calculated phase boundary between solid and liquid FeO₂H from (He et al., 2018). Also shown are the cold geotherm (Brown & Shankland, 1981) and hot geotherm (Anderson, 2002). The vertical bar represents the range of literature values for the CMB temperature (Nomura et al., 2014; Andrault et al., 2016).

3.2. EoS of FeO₂H_x solid and melt

We present the FPMD results on the equation of state and thermodynamic properties mainly focusing on the effects of hydrogen at high pressures. P phase was simulated at 300, 1000, 2000 and 3000 K. Its P-V results at 300 K are fit to a third-order Birch-Murnaghan equation of state (EoS) to obtain K_0 and K' with the reference volume and pressure fixed at the largest volume simulated (Birch, 1978). To represent the P-V data at elevated temperatures, we calculate the reference bulk modulus (K_{0T}) at the

corresponding temperatures by

255

256

257

258

259

260

261

262263

264

265266

267

268

269

270

271272

273

274

275

276

277

278

279

280

281

282

246
$$K_{0T} = K_0 + (\partial K / \partial T)_{0P} (T - 300)$$
 (1)

247 where $(\partial K/\partial T)_{0P}$ is the temperature derivative of the bulk modulus at the reference pressure. The reference volume (V_{0T}) at evaluated temperatures is expressed as

249
$$V_{0T} = V_0 \exp \int_{300}^{T} \alpha_T dT$$
 (2)

where α_T is the thermal expansion coefficient at high temperatures and the reference pressure and can be further written as

$$252 \alpha_T = \alpha_0 + \alpha_1 T (3)$$

where α_0 and α_1 are constants. The fitted parameters are summarized in the Table 1 and the results are plotted in Figure 3A.

Our 300 K isotherm calculated using GGA slightly lies above the high-pressure data (Nishi et al., 2017) and the deviation of volume is within ~0.5%. The experimental values seem to fall into two groups, the low-pressure group (< 90 GPa) and high-pressure group (> 90GPa). Similar trend can also be identified in a more recent experimental study (Yuan et al., 2018). We speculate that the dichotomy comes from the dehydrogenation of FeO₂H at high pressure. This speculation is supported by both experimental observations and calculations which show that FeO_2H_x (x < 1) is more stable at evaluated pressure and temperatures (e.g., He et al., 2018; Yuan et al., 2018). This also explains why most of first-principles studies "overestimate" volume compared with the high-pressure data by Nishi et al. (2017) (see Figure S4). On the other hand, even if no dehydrogenation occurs in the experiments of (Nishi et al., 2017), the isothermal bulk modulus K_T derived by fitting the experimental data directly does not differ much from our results. Within the thermal boundary layer (120 GPa to 136 GPa according to (Anderson, 2002)), the maximum difference for K_T is 2.5%, which corresponds to the difference in bulk sound velocity of 1.2% assuming that the density is the same. Such a small difference is insignificant for this study as shown in the following text.

As for the comparison with other calculations, our 300 K isotherm calculated using GGA almost overlaps with the two lowest pressure experimental data points on FeO₂H (Lu & Chen, 2018). The differences between GGA and GGA+U results are small (<1%) in the pressure range considered here (Figure S4). While GGA may not produce the correct electronic band gap (Jang et al., 2017; Streltsov et al., 2017), it produces the pressure-volume results, which are comparable to computationally more costly GGA+U results. Moreover, appropriate choice of U and U parameters is not clear. Therefore, we used GGA to calculate the isotherms of P phase and its liquid state.

For liquid FeO_2H_x , x can span from 0 to values greater than 1. x greater than 1 is possible only if the ambient mantle is enriched with hydrogen when melting occurs. Here we consider x = 0, 1, and 5, corresponding to hydrogen-depleted to hydrogen-enriched

conditions. Liquid FeO₂H was simulated at 3000, 4000, and 6000 K whereas liquid FeO₂ and FeO₂H₅ were performed at 4000 K (Figure 3B). The P-V-T results are described to the following expression (Karki et al., 2018),

$$P(V,T) = P(V,T_0) + B_{TH}(V)(T - T_0)$$
(4)

Here $P(V, T_0)$ represents the reference isotherm corresponding T_0 taken to be 3000 K, using a fourth-order Birch-Murnaghan equation of state and $B_{\rm TH}$ is defined as

$$B_{TH}(V) = \left[a - b(\frac{V}{V_0}) + c(\frac{V}{V_0})^2 \right] / 1000$$
 (5)

where a, b, and c are constants. The fitted parameters are summarized in Table 1.

The FPMD results show that both the temperature and hydrogen content increase the volume of liquid FeO_2H_x . The latter has much larger effects. Compared with solid FeO_2H , liquid FeO_2H is less dense for the entire pressure and temperature range considered (Figure 4A), as one would intuitively expect.

Using the pressure-volume-temperature-energy relationships obtained from the FPMD simulations, we can calculate the heat capacity at constant volume (C_V), thermal Gruneisen parameter (γ), and thermal expansivity (α) for both solid and liquid FeO₂H (Figure S5). Both liquid and solid FeO₂H are characterized with C_V larger than the Dulong–Petit limit (Figure S5A). γ of liquid FeO₂H gradually increases with pressure while γ of solid FeO₂H stays nearly constant at the pressures considered here (Figure S5B). Liquid FeO₂H as expected has larger thermal expansion coefficient than its solid counterpart (Figure S5C).

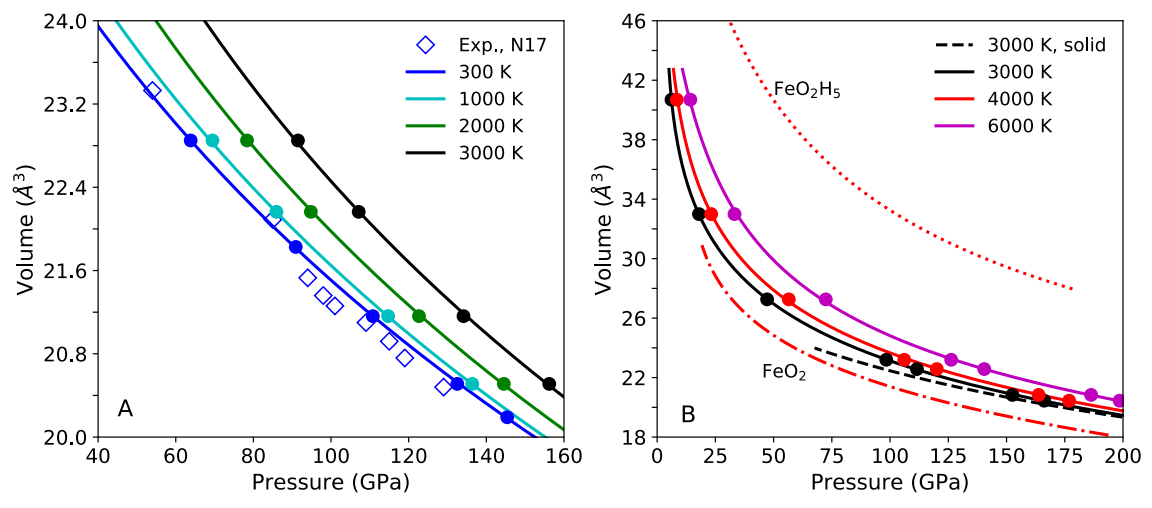


Figure 3. (A) Pressure-volume results of solid P phase at several temperatures (solid lines and solid circles), compared with experimental data at 300 K (open diamonds, N17)

(Nishi et al., 2017). **(B)** Pressure-volume results of FeO_2H liquid at 3000, 4000 and 6000 K (solid curves with circles). The equation of state of solid FeO_2H at 3000 K is shown for comparison (black dashed). Also shown are the calculated results at 4000 K for liquid FeO_2 (dotted dashed curve) and FeO_2H_5 (dotted curve).

Table 1. Fitted equation of state parameters for P phase, liquid FeO_2 , FeO_2H , and FeO_2H_5 . Uncertainties are given in parentheses.

	V ₀ (Å ³)	P ₀ (GPa)	T ₀ (K)	K ₀ (GPa)	K'	K" (1/GPa)	$\begin{array}{c} \alpha_0 \\ (10^{-6} \text{ K}^{-1}) \\ \text{or a} \end{array}$	$\begin{array}{c} \alpha_1 \\ (10^{-9} \text{ K}^{-2}) \\ \text{or b} \end{array}$	$(\partial K/\partial T)_{0P}$ (GPa K ⁻¹) or c
solid		63.8		545	3.0		8.9	7.4	-0.041
FeO ₂ H	22.85	(0.1)	300	(9)	(0.2)	n.a.	(0.5)	(0.4)	(0.001)
liquid		6.1		26	7.7	-0.71	22.2	25.5	5.9
FeO ₂ H	40.69	(0.1)	3000	(4)	(0.2)	(0.05)	(0.2)	(0.7)	(0.4)
liquid		23		92	7.1	-0.1605			
FeO_2	29.44	(0.1)	4000	(1)	(0.1)	(0.0004)	n.a.	n.a.	n.a.
liquid		33.5		136	2.7	-0.0079			
FeO ₂ H ₅	45.15	(0.1)	4000	(5)	(0.3)	(0.0003)	n.a.	n.a.	n.a.

^{*} a, b, c are dimensionless for the equation of state of liquid (Eq. 5)

The values of α and γ are necessary to calculate the adiabatic bulk modulus $(K_{\rm S})$ from the isothermal bulk modulus $(K_{\rm T})$, which can be readily evaluated with $K_T = -(\partial P/\partial \ln V)_T$. At lowermost mantle conditions, α and γ of both liquid and solid FeO₂H vary marginally (Figure S5B, C). We thus choose $\alpha = 2 \times 10^{-5}~{\rm K}^{-1}$, $\gamma = 1.7$ for liquid FeO₂H and $\alpha = 1.5 \times 10^{-5}~{\rm K}^{-1}$, $\gamma = 1.8$ for solid FeO₂H to calculate $K_{\rm S}$ around CMB conditions using $K_S = K_T(1 + \alpha \gamma T)$. For sake of simplicity, we also assume that liquid FeO₂ and FeO₂H₅ have the same α and γ as FeO₂H. Furthermore, the bulk sound velocity (V_{ϕ}) can be evaluated by $V_{\phi} = \sqrt{K_S/\rho}$, where ρ is the density (Figure 4B). Our V_{ϕ} of pyrite-type FeO₂H at 300 K and 3000 K agrees well with (Liu et al., 2017) within uncertainties, considering x of 0.5-0.7 in (Liu et al., 2017). An increase in x has been suggested to increase the sound velocity of P phase (Liu et al., 2017; Huang et al., 2018). Similar to density, the sound velocity of liquid FeO₂H is much lower than that of its solid counterpart. The sound velocity of liquid FeO₂H_x also strongly depends on the hydrogen content (Figure 4A).

^{*} n.a. means not applicable

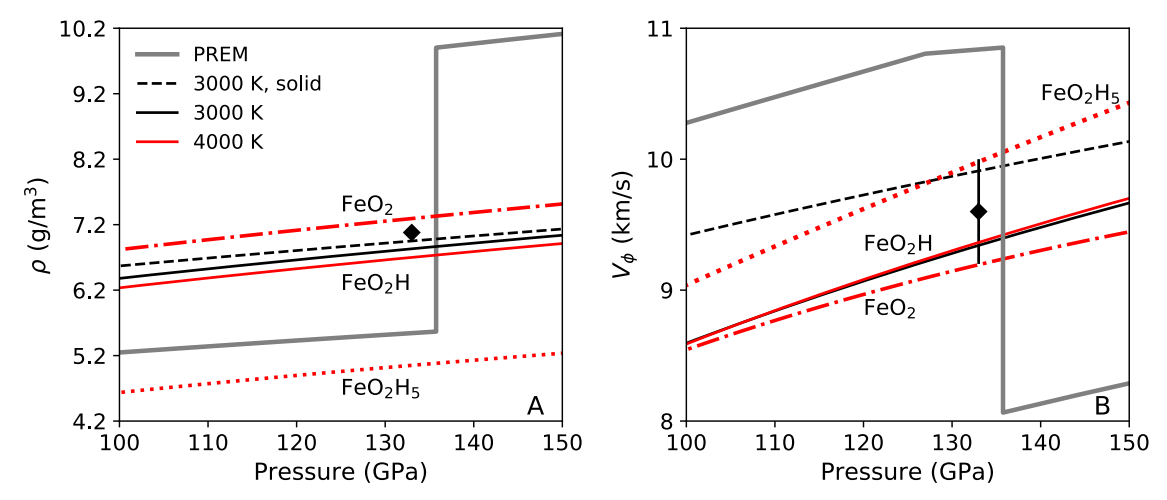


Figure 4. (A) Density and **(B)** bulk sound velocity of FeO₂H melt at 3000 and 4000 K (solid curves), and P phase at 3000 K (dashed line). The results for FeO₂ and FeO₂H₅ liquids are at 4000 K. Density and bulk sound velocity of PREM model (Dziewonski & Anderson, 1981) and experimental data (diamond) on the bulk sound velocity of FeO₂H_x at ~2600 K (Liu et al., 2017) are plotted for comparison. Legend is the same for A and B.

4. Implications for ULVZs

339 340

341342

343

344

345346347

348349

350

351

352

353

354

355

356

357

358

359

360

361362

363

364365

366

367

368

369

370

371

372

Our first principles results suggest that P phase is unlikely to be the source material of ULVZs based on its relatively low melting temperature. However, liquid FeO₂H_x may be a potential provenance of ULVZs. First, liquid FeO₂H_x is characterized with very low seismic velocity. Its V_{ϕ} is much lower than the velocity of the isochemical solid and the ambient mantle (Figure 4B). As a result, assuming the Voigt average, a mixture of ~20% (by volume) liquid FeO₂H and the ambient mantle can reproduce the seismic observations in ULVZs, while for pyrite-type FeO₂H ~60%–70% of P phase is required (Huang et al., 2018). Given that FeO₂H_x is a minor mineral in the subducted slabs and also may be partly consumed during the course of subduction by reacting with other volatiles such as CO₂ (Boulard et al., 2018), a smaller demand on the amount of delivered FeO₂H_x favors the hypothesis of FeO₂H_x-induced ULVZs. The 20% liquid FeO₂H within the ULVZs could be generated by the reaction of the unlimited iron reservoir in the core and the water brought by subduction from the crust and the primordial water in the mantle (Hallis et al., 2015) as originally proposed (Liu et al., 2017; Mao et al., 2017). Second, liquid FeO_2H_x could be maintained in the ambient mantle without drainage. The density of liquid FeO₂H_x is very sensitive to the hydrogen content (Figure 4A). A linear interpolation shows that liquid FeO_2H_x could be neutrally buoyant if x = -3, that is, FeO₂H_x contains -3.3 wt% hydrogen. In this case, liquid FeO₂H_x could mix with the ambient mantle free of gravitational separation.

However, such a large amount of H is difficult to justify, since P phase tends to release hydrogen at elevated temperatures (Liu et al., 2017; Yuan et al., 2018). For $0 \le x$ <1, the FeO₂ melt is quite dense (Figure 4A), but the melt viscosity is likely to be negligibly small compared with solid ambient mantle (Karki & Stixrude, 2010). To maintain such a dense melt within the solid mixture against compaction is difficult

(Karato, 2014). Yet, this is still achievable provided that the topography of the ULVZ region is maintained by the pressure gradient caused by the convective current above that region, as proposed by (Hernlund & Jellinek, 2010). The degree to which convective stirring keeps melt in a layer can be evaluated by a non-dimensional ability parameter, R $=\Delta\rho gH^2/\eta v$, where $\Delta\rho$ is the density difference between the melt and solid matrix, η is the viscosity of the solid matrix, H, η and v are the height, viscosity, and convective velocity of ULVZ, respectively (Jellinek & Manga, 2004; Hernlund & Jellinek, 2010). If $R \ll 1$, convective stirring dominates and a substantial amount of melt could be maintained in a layer. Assuming H = 10 km (the typical thickness of a ULVZ) (Bower et al., 2011) and the solid matrix is composed of the same material as the ambient mantle, R as a function η and ν is estimated (Figure 5A) for two different $\Delta \rho$, i.e., the density differences between FeO₂ or FeO₂H and the ambient mantle. The ability for a convective pressure gradient to stir melt (R) critically hinges on η and v and is relatively insensitive to the density of liquid itself. Unfortunately, η and ν of solid matrix of ULVZs are not well constrained. The estimates of η range from 10^{18} to 10^{21} Pa s (Nakada & Karato, 2012; Forte et al., 2015). The typical mantle convection rate is 10⁻⁹ m/s. If the material circulation rate within the ULVZs is of the same order of this value, stirring is unlikely even if the viscosity is 10^{21} Pa s, unless the ULVZs are very thin (< 6 km) (Figure 5B). However, near the ULVZ region where a large density anomaly likely exists, much larger velocities may be possible (Karato, 2014). In this case, dense FeO₂H_x melt may be kept within the ULVZs.

373

374

375

376

377378

379

380

381

382

383

384

385

386

387

388

389 390

391

392

393

394395

396 397 398

399

400

401

402

403 404

405

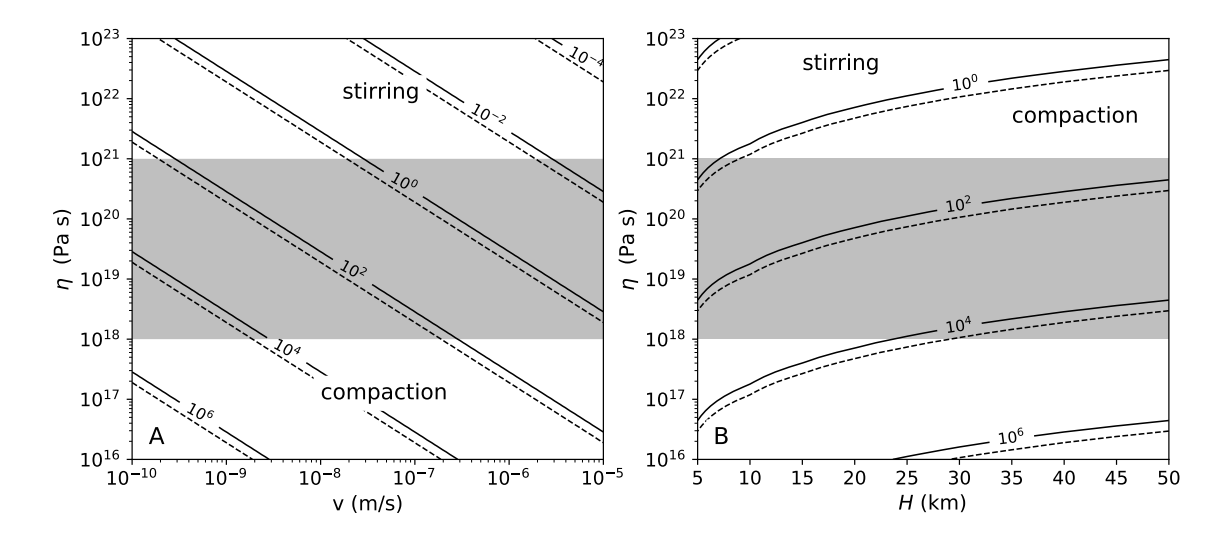


Figure 5. The ability factor (R) for a convective pressure gradient to stir melt to maintain a ULVZ dynamically stable. (**A**) R as function of the viscosity of the solid matrix (η) and the convecting rate of ULVZs materials (ν) for two different melts, FeO₂ (solid contours) and FeO₂H (dashed contours) assuming the thickness of the ULVZ (H) is 10 km. (**B**) R as function of the viscosity of the solid matrix (η) and the thickness of ULVZs at a typical convecting rate of ULVZs materials ($\nu = 10^{-9}$ m/s). R = 1 divides the parameter space into two regions, i.e., compaction dominant (R > 1) and stirring dominant (R < 1). The shaded bar represents the literature values of mantle viscosity near CMB (Nakada & Karato, 2012; Forte et al., 2015).

5. Conclusions

We estimated the congruent melting temperatures of both pyrite-type FeO₂H and FeO₂ using first-principles molecular dynamics method. Our results suggest that P phase, whether it is brought down in to the deep mantle by subducted slabs or formed in the lowermost mantle in some other way (Mao et al., 2017), is likely to melt and remain molten near the CMB where ULVZs are located. Our results also suggest that the sound velocity of liquid FeO₂H is much lower than the pyrite-type FeO₂H at the same conditions, thus requiring smaller amounts of FeO₂H liquid to induce the same amount of seismic reduction in ULVZs.

If a ULVZ is indeed composed of a FeO₂H_x melt-bearing slurry, it would be meltenriched near the top relative to the bottom (Hernlund & Jellinek, 2010) and consequently exhibits the positive gradient in seismic shear velocities, consistent with seismic observations (Rost et al., 2006). However, it requires certain special physical conditions in order to maintain such slurry against compaction. Specifically, these conditions are that hydrogen is extremely enriched (x = -3), or if x is small (x < 3) the viscosity of the surrounding solid matrix is very viscous and/or ULVZs convect much more vigorously compared with the rest of the mantle.

Acknowledgments

We thank Felipe González-Cataldo and Qijun Hong for discussions. We are grateful to the two anonymous reviewers for very useful comments and suggestions that improved the manuscript. The research is supported by NSF grants (EAR-1321956 and EAR-1551348) to K. K. M. Lee, (EAR 1764140) to B. B. Karki. We thank the Yale Center for Research Computing for guidance and use of the research computing infrastructure, specifically Kaylea Nelson. High performance computing resources were also provided by Louisiana State University.

Reference:

- Anderson, O. (1982). The Earth's Core and the Phase-Diagram of Iron. *Philosophical Transactions of the Royal Society a-Mathematical Physical and Engineering Sciences*, 306(1492), 21-35. https://doi.org/10.5636/jgg.45.1235
- Anderson, O. (2002). The power balance at the core—mantle boundary. *Physics of the Earth and Planetary Interiors*, 131(1), 1-17. https://doi.org/10.1016/S0031-9201(02)00009-2
- Andrault, D., Monteux, J., Le Bars, M., & Samuel, H. (2016). The deep Earth may not be cooling down. *Earth and Planetary Science Letters*, *443*, 195-203. https://doi.org/10.1016/j.epsl.2016.03.020
- Belonoshko, A. B., & Rosengren, A. (2012). High-pressure melting curve of platinum from ab initio Z method. *Physical Review B*, 85(17), 174104.
- 452 https://doi.org/10.1103/PhysRevB.85.174104

- 453 Belonoshko, A. B., Skorodumova, N. V., Rosengren, A., & Johansson, B. (2006).
- Melting and critical superheating. *Physical Review B*, 73(1), 012201.
- 455 https://doi.org/10.1103/PhysRevB.73.012201
- 456 Birch, F. (1978). Finite strain isotherm and velocities for single-crystal and
- polycrystalline NaCl at high pressures and 300°K. *Journal of Geophysical Research*:
- 458 Solid Earth, 83(B3), 1257-1268. https://doi.org/10.1029/JB083iB03p01257
- Blöchl, P. E., Jepsen, O., & Andersen, O. K. (1994). Improved tetrahedron method for Brillouin-zone integrations. *Physical Review B*, *49*(23), 16223-16233. https://doi.org/10.1103/PhysRevB.49.16223
- Boulard, E., Guyot, F., Menguy, N., Corgne, A., Auzende, A.-L., Perrillat, J.-P., & Fiquet, G. (2018). CO₂-induced destabilization of pyrite-structured FeO₂H_x in the lower mantle. *National Science Review*, nwy032-nwy032.
- https://doi.org/10.1093/nsr/nwy032
- Bower, D. J., Wicks, J. K., Gurnis, M., & Jackson, J. M. (2011). A geodynamic and
 mineral physics model of a solid-state ultralow-velocity zone. *Earth and Planetary Science Letters*, 303(3-4), 193-202.
- Brown, J., & Shankland, T. J. (1981). Thermodynamic Parameters in the Earth as
 Determined from Seismic Profiles. *Geophysical Journal of the Royal Astronomical* Society, 66(3), 579-596. https://doi.org/10.1111/j.1365-246X.1981.tb04891.x
- Brown, S., Thorne, M. S., Miyagi, L., & Rost, S. (2015). A compositional origin to
 ultralow-velocity zones. *Geophysical Research Letters*, 42(4), 1039-1045.
 https://doi.org/10.1002/2014GL062097
- Deemyad, S., & Silvera, I. F. (2008). Melting Line of Hydrogen at High Pressures.
 Physical Review Letters, 100(15), 155701.
 https://doi.org/10.1103/PhysRevLett.100.155701
- Deng, J., Du, Z., Benedetti, L. R., & Lee, K. K. M. (2017). The influence of wavelength-dependent absorption and temperature gradients on temperature determination in laser-heated diamond-anvil cells. *Journal of Applied Physics*, *121*(2), 025901. https://doi.org/10.1063/1.4973344
- Dziewonski, A. M., & Anderson, D. L. (1981). Preliminary reference Earth model.

 Physics of the Earth and Planetary Interiors, 25(4), 297-356.

 https://doi.org/10.1016/0031-9201(81)90046-7
- Fischer, R. A., & Campbell, A. J. (2010). High-pressure melting of wüstite. *American Mineralogist*, *95*(10), 1473-1477. https://doi.org/10.2138/am.2010.3463
- Forte, A. M., Simmons, N. A., & Grand, S. P. (2015). 1.27 Constraints on Seismic
 Models from Other Disciplines Constraints on 3-D Seismic Models from Global
 Geodynamic Observables: Implications for the Global Mantle Convective Flow A2 Schubert, Gerald. In *Treatise on Geophysics (Second Edition)* (pp. 853-907). Oxford:
- 491 Elsevier. https://doi.org/10.1016/B978-0-444-53802-4.00028-2
- Ghosh, D. B., & Karki, B. B. (2016). Solid-liquid density and spin crossovers in (Mg,
 Fe)O system at deep mantle conditions. *Scientific Reports*, 6, 37269.
 https://doi.org/10.1038/srep37269
- González-Cataldo, F., Davis, S., & Gutiérrez, G. (2016). Melting curve of SiO₂ at multimegabar pressures: implications for gas giants and super-Earths. *Scientific*
- 497 Reports, 6, 26537. https://doi.org/10.1038/srep26537

- Hallis, L. J., Huss, G. R., Nagashima, K., Taylor, G. J., Halldórsson, S. A., Hilton, D. R.,
 et al. (2015). Evidence for primordial water in Earth's deep mantle. *Science*,
- 500 350(6262), 795-797. https://doi.org/10.1126/science.aac4834
- He, Y., Kim, D. Y., Pickard, C. J., Needs, R. J., Hu, Q., & Mao, H.-k. (2018). Superionic
 hydrogen in Earth's deep interior. *arXiv e-prints*. Retrieved from
 https://ui.adsabs.harvard.edu/-abs/2018arXiv181008766H
- Hernlund, J. W., & Jellinek, A. M. (2010). Dynamics and structure of a stirred partially molten ultralow-velocity zone. *Earth and Planetary Science Letters*, *296*(1), 1-8. https://doi.org/10.1016/j.epsl.2010.04.027
- Hu, Q. Y., Kim, D. Y., Liu, J., Meng, Y., Yang, L. X., Zhang, D. Z., et al. (2017).
 Dehydrogenation of goethite in Earth's deep lower mantle. *Proceedings of the National Academy of Sciences of the United States of America*, 114(7), 1498-1501.
 https://doi.org/10.1073/pnas.1620644114
- Huang, S., Qin, S., & Wu, X. (2018). Elasticity and Anisotropy of the Pyrite-Type FeO₂H-FeO₂ System in Earth's Lowermost Mantle. *Journal of Earth Science*. https://doi.org/10.1007/s12583-018-0836-y
- Jang, B. G., Kim, D. Y., & Shim, J. H. (2017). Metal-insulator transition and the role of electron correlation in FeO₂. *Physical Review B*, *95*(7), 075144. https://doi.org/10.1103/PhysRevB.95.075144
- Jellinek, A. M., & Manga, M. (2004). Links between long-lived hot spots, mantle plumes, D", and plate tectonics. *Reviews of Geophysics*, 42(3). https://doi.org/10.1029/2003RG000144
- Karato, S.-i. (2014). Does partial melting explain geophysical anomalies? *Physics of the Earth and Planetary Interiors*, 228, 300-306.
 https://doi.org/10.1016/j.pepi.2013.08.006
- Karki, B. B., Ghosh, D. B., Maharjan, C., Karato, S.-i., & Park, J. (2018). Density Pressure Profiles of Fe-Bearing MgSiO3 Liquid: Effects of Valence and Spin States,
 and Implications for the Chemical Evolution of the Lower Mantle. *Geophysical Research Letters*, 45(9), 3959-3966. https://doi.org/10.1029/2018GL077149
- Karki, B. B., & Stixrude, L. P. (2010). Viscosity of MgSiO₃ Liquid at Earth's Mantle
 Conditions: Implications for an Early Magma Ocean. *Science*, *328*(5979), 740-742.
 https://doi.org/10.1126/science.1188327
- Kresse, G., & Joubert, D. (1999). From ultrasoft pseudopotentials to the projector augmented-wave method. *Physical Review B*, *59*(3), 1758-1775. https://doi.org/10.1103/PhysRevB.59.1758
- Li, D., Zhang, P., & Yan, J. (2014). Ab initio molecular dynamics study of high-pressure melting of beryllium oxide. *Scientific Reports*, *4*, 4707. https://doi.org/10.1038/srep04707
- Lin, J.-F., Gregoryanz, E., Struzhkin, V. V., Somayazulu, M., Mao, H.-k., & Hemley, R. J. (2005). Melting behavior of H2O at high pressures and temperatures. *Geophysical Research Letters*, *32*(11). https://doi.org/doi:10.1029/2005GL022499
- Liu, J., Hu, Q., Young Kim, D., Wu, Z., Wang, W., Xiao, Y., et al. (2017). Hydrogen-bearing iron peroxide and the origin of ultralow-velocity zones. *Nature*, *551*, 494.
- https://doi.org/https://doi.org/10.1038/nature24461

- Lu, C., & Chen, C. (2018). High-Pressure Evolution of Crystal Bonding Structures and Properties of FeOOH. *The Journal of Physical Chemistry Letters*, 2181-2185.
- 544 https://doi.org/10.1021/acs.jpclett.8b00947
- Mao, H., Hu, Q., Yang, L., Liu, J., Kim, D. Y., Meng, Y., et al. (2017). When water meets iron at Earth's core—mantle boundary. *National Science Review*, *4*(6), 870-878. https://doi.org/10.1093/nsr/nwx109
- Mao, W. L., Mao, H.-k., Sturhahn, W., Zhao, J., Prakapenka, V. B., Meng, Y., et al.
 (2006). Iron-Rich Post-Perovskite and the Origin of Ultralow-Velocity Zones. *Science*,
 312(5773), 564-565. https://doi.org/10.1126/science.1123442
- Mashino, I., Murakami, M., & Ohtani, E. (2016). Sound velocities of δ-AlOOH up to
 core-mantle boundary pressures with implications for the seismic anomalies in the
 deep mantle. *Journal of Geophysical Research: Solid Earth*, 121(2), 595-609.
 https://doi.org/doi:10.1002/2015JB012477
- Nakada, M., & Karato, S. (2012). Low viscosity of the bottom of the Earth's mantle inferred from the analysis of Chandler wobble and tidal deformation. *Physics of the Earth and Planetary Interiors*, 192, 68-80. https://doi.org/10.1016/J.Pepi.2011.10.001
- Nishi, M., Kuwayama, Y., Tsuchiya, J., & Tsuchiya, T. (2017). The pyrite-type high-pressure form of FeOOH. *Nature*, *547*, 205. https://doi.org/10.1038/nature22823
- Nomura, R., Hirose, K., Uesugi, K., Ohishi, Y., Tsuchiyama, A., Miyake, A., & Ueno, Y. (2014). Low Core-Mantle Boundary Temperature Inferred from the Solidus of Pyrolite. *Science*, *343*(6170), 522-525. https://doi.org/10.1126/science.1248186
- Nomura, R., Ozawa, H., Tateno, S., Hirose, K., Hernlund, J., Muto, S., et al. (2011). Spin crossover and iron-rich silicate melt in the Earth/'s deep mantle. *Nature*, 473(7346), 199-202. https://doi.org/10.1038/nature09940
- Perdew, J. P., Burke, K., & Ernzerhof, M. (1996). Generalized Gradient Approximation
 Made Simple. *Physical Review Letters*, 77(18), 3865-3868.
 https://doi.org/10.1103/PhysRevLett.77.3865
- Rost, S., Garnero, E. J., & Williams, Q. (2006). Fine-scale ultralow-velocity zone
 structure from high-frequency seismic array data. *Journal of Geophysical Research: Solid Earth*, 111(B9). https://doi.org/doi.10.1029/2005JB004088
- 572 Streltsov, S. S., Shorikov, A. O., Skornyakov, S. L., Poteryaev, A. I., & Khomskii, D. I. (2017). Unexpected 3+ valence of iron in FeO₂, a geologically important material lying "in between" oxides and peroxides. *Scientific Reports*, 7(1), 13005. https://doi.org/10.1038/s41598-017-13312-4
- Tang, M., Niu, Z.-W., Zhang, X.-L., & Cai, L.-C. (2018). Structural stability of FeO2 in
 the pressure range of lower mantle. *Journal of Alloys and Compounds*, 765, 271-277.
 https://doi.org/https://doi.org/10.1016/j.jallcom.2018.06.237
- Wang, S., Zhang, G., Liu, H., & Song, H. (2013). Modified Z method to calculate
 melting curve by molecular dynamics. *The Journal of Chemical Physics*, 138(13),
 134101. https://doi.org/10.1063/1.4798225
- Wicks , J. K., Jackson, J. M., & Sturhahn, W. (2010). Very low sound velocities in iron rich (Mg,Fe)O: Implications for the core-mantle boundary region. *Geophysical Research Letters*, *37*(15), L15304. https://doi.org/10.1029/2010GL043689
- Williams, Q., & Garnero, E. J. (1996). Seismic Evidence for Partial Melt at the Base of Earth's Mantle. *Science*, 273(5281), 1528-1530.
- 587 https://doi.org/10.1126/science.273.5281.1528

Yuan, L., Ohtani, E., Ikuta, D., Kamada, S., Tsuchiya, J., Naohisa, H., et al. (2018). 588 589 Chemical Reactions Between Fe and H2O up to Megabar Pressures and Implications 590 for Water Storage in the Earth's Mantle and Core. Geophysical Research Letters, n/a-591 n/a. https://doi.org/10.1002/2017GL075720 592 Zhang, L., Yuan, H., Meng, Y., & Mao, H.-k. (2018). Discovery of a hexagonal 593 ultradense hydrous phase in (Fe,Al)OOH. Proceedings of the National Academy of 594 Sciences. https://doi.org/10.1073/pnas.1720510115 595 Zhang, X.-L., Niu, Z.-W., Tang, M., Zhao, J.-Z., & Cai, L.-C. (2017). First-principles 596 thermoelasticity and stability of pyrite-type FeO₂ under high pressure and temperature. 597 Journal of Alloys and Compounds, 719, 42-46. 598 https://doi.org/10.1016/j.jallcom.2017.05.143 599